Electronic and Molecular Structures of Trigonal Truxene-Core Systems Conjugated to Peripheral Fluorene Branches. Spectroscopic and Theoretical Study

ARTICLE *in* THE JOURNAL OF PHYSICAL CHEMISTRY B · APRIL 2007

Impact Factor: 3.3 · DOI: 10.1021/jp065271w · Source: PubMed

7 AUTHORS, INCLUDING:

Juan Casado
University of Malaga
227 PUBLICATIONS **3,688** CITATIONS
SEE PROFILE

Juan Teodomiro López Navarrete
University of Malaga
335 PUBLICATIONS **5,249** CITATIONS
SEE PROFILE

Peter Skabara
University of Strathclyde
194 PUBLICATIONS **3,164** CITATIONS
SEE PROFILE

Igor F Perepichka
Bangor University
125 PUBLICATIONS **3,148** CITATIONS
SEE PROFILE

Electronic and Molecular Structures of Trigonal Truxene-Core Systems Conjugated to Peripheral Fluorene Branches. Spectroscopic and Theoretical Study

María Moreno Oliva, Juan Casado, and Juan T. López Navarrete*

Departamento de Química Física, Universidad de Málaga, Campus de Teatinos s/n, Málaga 29071, Spain

Rory Berridge

Department of Chemistry, University of Manchester, Manchester M1 9PL, United Kingdom

Peter J. Skabara and Alexander L. Kanibolotsky

WestCHEM, Department of Pure and Applied Chemistry, University of Strathclyde, Glasgow G1 1XL, United Kingdom

Igor F. Perepichka

L. M. Litvinenko Institute of Physical Organic and Coal Chemistry, National Academy of Sciences of Ukraine, Donetsk 83114, Ukraine

Received: August 15, 2006; In Final Form: February 15, 2007

An analysis is performed on the molecular and electronic features in a series of trigonal molecules constituted by a central truxene core which is ramified with three oligofluorene moieties of different lengths. Arms and core are studied independently and upon threefold unification. Special emphasis is paid to the modulation of the conjugational properties in relation to substitution, molecular dimension, ring aromaticity, intermolecular forces, oxidation state, etc. Raman and optical absorption/emission spectroscopies in conjunction with computational theoretical results are combined for this purpose. The evolution of some key intensity ratios in the Raman spectra (i.e., I_{1300}/I_{1235}) is followed as an indication of electronic interaction between the core and the branches. The changes of the electronic delocalization upon solvation, with varying temperature in the solid state, with the nature of the aromatic unit (bithiophene/fluorene) or after electrochemical oxidation are interpreted. The modulation of the optical properties on the basis of the structure and energetics of the orbital around the gap is also addressed. Density functional theory was used to assign the vibrational and electronic spectra.

I. Introduction

The field of well-defined π-conjugated oligomers is today recognized as a prominent prospect in materials science. In this field, linearly (i.e., one-dimensional) conjugated molecules constitute a fruitful area of research.[1] Recently, star-shaped conjugated oligomers have attracted tremendous interest,[2] particularly because they expand the potential of linear analogues in electronic, optoelectronic, and photonic applications [i.e., light-emitting diodes (LED),[3] photovoltaics,[4] field-effect transistors (FET),[5] third-order nonlinear optics,[6] etc.]. The possibility of extending the electronic structure in two dimensions leads to the realization of organic molecules built with peripheral antennae converging to a central core for energy conversion (i.e., light-harvesting systems).[4] Conversely, these new star-shaped or dendrimer-like molecules, if constructed with fluorescent blocks, can be viewed as condensates of more efficient or highly emitting systems.[3] In this context, the precise elucidation of the interplay between the energy and electronic states of the core and of the external branches is of relevance for improved designs.

Polyfluorenes have emerged as leading electroluminescent materials with bright emission, high hole mobility, and ease of functionalization for tuning properties.[7,8] Their oligomeric homologues (i.e., oligofluorenes) serve as good models for photophysical studies and offer a greater degree of chemical purity, structural uniformity, or resistance to degradation, crucial factors for the performance of their LED devices.[9] Oligofluorene units have recently been used as arms in star-shaped architectures with various cores.[2h,3b−d,h,10] 10,15-Dihydro-5*H*-diindeno-[1,2-*a*;1′,2′-*c*]fluorene (truxene), a polycyclic aromatic system with C_3 symmetry, has been used as a potential starting material for the construction of bowl-shaped fragments of fullerenes, C_3 tripodal materials in chiral recognition, and liquid crystalline compounds.[11] Recently truxene has been recognized as a promising building block in conjugated star-shaped and dendritic architectures and potentially interesting for optoelectronic applications.[2e,5b,10,12] Truxene can be viewed as three "overlapped" fluorene fragments, which is an excellent choice as a core for the visualization of star-shaped oligofluorenes.

In this work, we describe the molecular and electronic structure of a series of trigonal star-shaped oligofluorenes having truxene as the central core and up to quaterfluorene arms (see Figure 1), resulting in nanosized macromolecules with ca. 4 nm radius.[10] The 9-positions of the fluorene units are substituted with hexyl chains for improving solubility and processability. A combination of molecular spectroscopies (i.e., vibrational

10.1021/jp065271w CCC: $37.00
Published on Web 04/03/2007

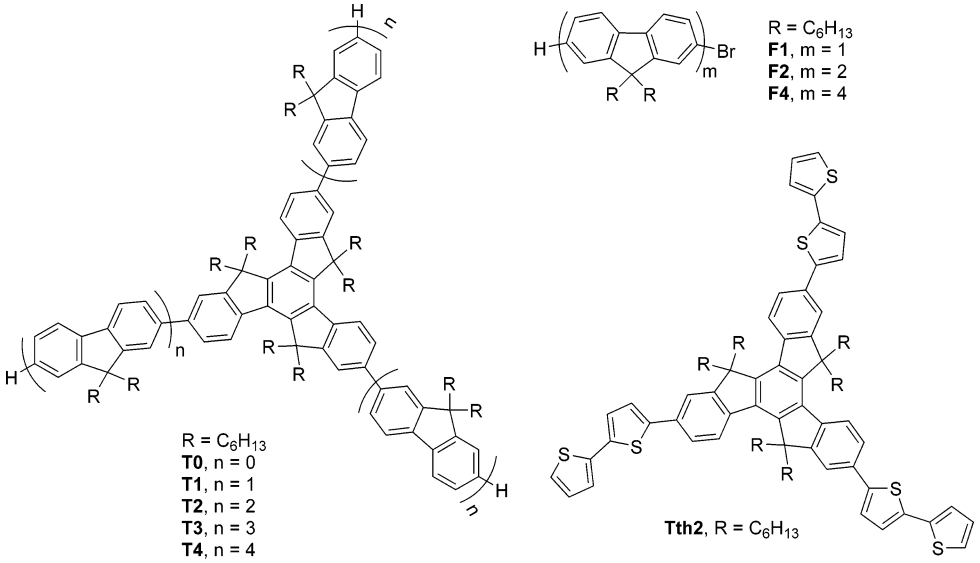

Figure 1. Chemical structures of the compounds studied: **T0**−**T4**, **F1**−**F4**, and **Tth2**. In theoretical calculations of truxene and fluorene derivatives, methyl (R = CH_3) instead of hexyl (R = C_6H_{13}) groups have been considered. In addition, calculations for fluorene series **F1**, **F2**, and **F4** have been performed for structures with a hydrogen atom instead of bromine.

Raman and absorption/emission) and theoretical calculations (density functional theory) is used to explore the electronic and molecular properties as a function of (i) substitution of truxene, (ii) core-to-arms electronic delocalization, (iii) length of the branches, (iv) intermolecular interactions, and (v) solid-state packing by means of thermospectroscopy.

Vibrational Raman spectroscopy is well suited for studying the electronic coupling between covalently connected conjugated moieties. This suitability lies in the important enhancement of the Raman activity for those vibrational modes that vibronically couple the electronic structure of the ground electronic state and the first accessible dipole-allowed excited state.[13] The coupling between electronic and vibrational degrees of freedom might strongly affect the nature of the photoexcitations; hence the rationalization of this behavior would help to optimize photophysical properties. In this sense Raman spectra (i.e., peak position and intensity of the relevant lines) as a function of the substitution pattern might be useful in estimating electronic delocalization (i.e., to what extent different moieties π-interact). Electronic spectra, on the other hand, constitute the means for investigating the electronic structure, emphasizing the relative disposition of the electronic levels and energy gap upon molecular trigonalization. The understanding of the underlying structure−property relationships is the driving force for executing this work, with the aim of offering information for the design of new conjugated systems.

II. Experimental and Computational Details

The syntheses of all the compounds studied have been reported previously.[10] Electrochemical oxidation was performed on thin solid films at room temperature in a 0.1 M tetrabutylammonium hexafluorophosphate solution in dry and oxygen-free acetonitrile. Platinum disk and platinum foil were used as working and auxiliary electrodes, and Ag wire was used as a pseudoreference electrode. Electrolysis conditions were tested against the Fc/Fc^+ couple as an internal reference. The procedure involved the immersion of the oligomer film (drop-cast on the Pt working electrode) in the electrolyte solution followed by application of an anodic potential according to previously reported cyclic voltammetry data.[10] Upon full oxidation, the Raman spectra were directly recorded in situ on the coated Pt electrode. The experiments were carried out using Voltalab40 electrochemical equipment from Radiometer.

Absorption and emission spectra were obtained in dichloromethane solution in concentrations (ca. 10^{-6}−10^{-7} M) not exceeding 0.1 au of absorbance (1 cm path length cell). Under these conditions, the absorption intensity was found to have linear dependence with concentration. There was no shift in the absorption wavelengths, indicating no aggregation in the system. UV−vis−NIR absorption spectra were recorded on an Agilent 8453 instrument equipped with a diode array detection system. Emission spectra were measured using a JASCO FP-750 spectrofluorometer. No fluorescent contaminants were detected upon excitation in the wavelength region of experimental interest. FT-Raman spectra were measured using an FT-Raman accessory kit (FRA/106-S) of a Bruker Equinox 55 FT-IR interferometer. A continuous-wave Nd:YAG laser working at 1064 nm was employed for excitation. A germanium detector operating at liquid nitrogen temperature was used. Raman scattering radiation was collected in a backscattering configuration with a standard spectral resolution of 4 cm^{-1}. To avoid possible damage to the oxidized samples upon laser radiation, its power was kept at a level lower than 20 mW and 1000−3000 scans were averaged for each spectrum. Raman spectra in solution were obtained in analytical grade CH_2Cl_2. A variable-temperature cell Specac P/N 21525 was used to record the FT-Raman spectra at different temperatures. This cell consists of a surrounding vacuum jacket (0.5 Torr) and combines a refrigerant Dewar and a heating block as the sample holder, allowing achievement of temperatures between −170 and +150 °C. Samples were inserted into the heating block part or the Dewar/cell holder assembly as a solid in a quartz cell and Raman spectra were recorded after waiting for thermal equilibrium of the sample, which required 20 min for every increment of 10 °C.

Density functional theory (DFT) methods have become very popular since the inclusion of electron correlation effects with accuracies comparable to those of correlated ab initio procedures, such as MP2, while reducing substantially the computational costs of the latter.[14] Hence, the use of low-cost computational DFT procedures has demonstrated very satisfactory results for conjugated molecules where electron correlation

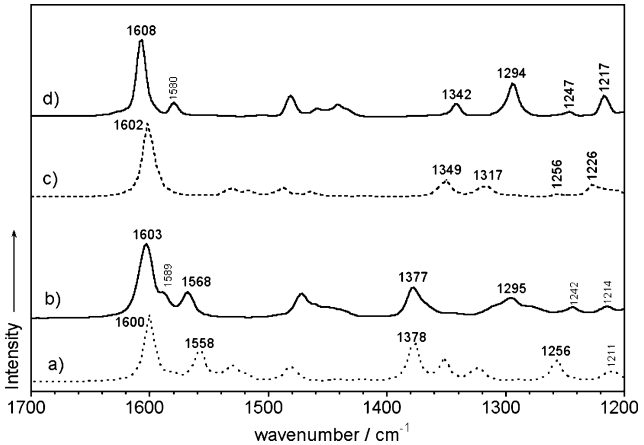

Figure 2. Comparison of (a) B3LYP/3-21G* theoretical and (b) solid-state Raman spectra of truxene **T0** and (c) B3LYP/3-21G* theoretical and (d) solid-state Raman spectrum of fluorene **F1**. For the theoretical spectra, methyl groups instead of hexyl groups have been considered.

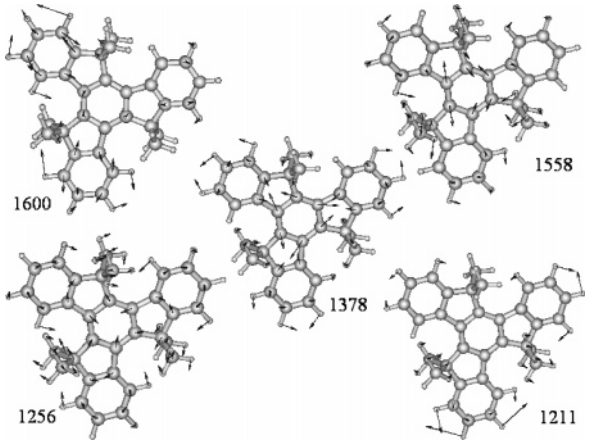

Figure 3. B3LYP/3-21G* theoretical eigenvector for some representative bands of **T0**.

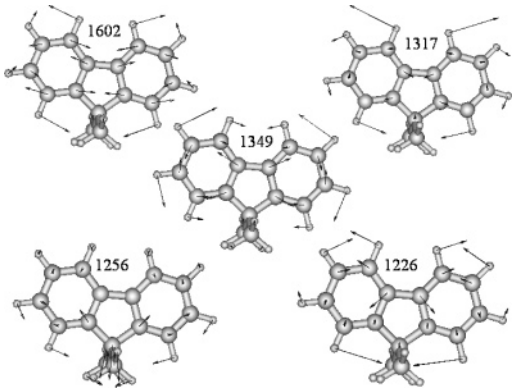

Figure 4. B3LYP/3-21G* theoretical eigenvector for some representative bands of **F1**.

plays a decisive role. Ground-state total energies, equilibrium geometries, eigenfrequencies, and normal coordinates were calculated using density functional theory by means of the Gaussian 03 package of programs.[15] The Becke's three parameter (B3) gradient-corrected exchange functional combined with the correlation Lee−Yang−Parr (LYP) functional was utilized.[16] The 3-21G* basis set was used.[17] Details of the modeling experiments are as follows: (i) Optimal geometries were determined on isolated entities, and neither solvent nor counteranion effects were considered. (ii) All the geometrical parameters were left to vary independently during the optimization. In the case of the conformational study, the dihedral angle between the fluorene units in **F2** was kept constant. Eventually, methyl groups instead of hexyl chains were considered, assuming that this substitution has a negligible affect on conjugation and the energies of the frontier orbitals. For **F2** Raman spectra calculations, the entire molecular structure was considered. (iii) For the theoretical Raman spectra of the resulting ground-state optimized geometries, harmonic vibrational frequencies and Raman intensities were calculated numerically. (iv) Ab initio calculations can be expected to yield vibrational frequencies with an accuracy of about 10% compared to the respective experimental values.[18] To improve the numerical comparison, calculated harmonic vibrational frequencies are uniformly scaled down by a random factor (0.97) to best fit the experimental quantities. All quoted theoretical vibrational frequencies reported are thus scaled values.

The time-dependent DFT (TD-DFT) approach is now being widely applied in both chemistry and condensed matter physics to describe electronic excitations.[19] While it is not as accurate for excitations as the ordinary DFT is for ground-state properties, this theory has a considerable predictive power and is computationally quite tractable. At least 30 lowest energy electronic excited states were computed for all the molecules. TD-DFT calculations were performed using the same functional (B3LYP) and basis set (3-21G*).

III. Molecular Structures. Raman Spectra: Structure−Spectra Correlations

III.1. Raman Spectrum of Truxene and Fluorene Building Blocks. Figure 2 compares the FT-Raman spectra of **T0** and **F1** together with their B3LYP/3-21G* theoretical data. The focus of this analysis concerns CC skeletal vibrations because of their direct implication in the coupling between the molecular and electronic structures.[13] For the 1600−1200 cm^{-1} region, a relatively good experimental/theoretical correlation is noticed for both compounds, which allows us to investigate and assign the principal experimental bands of the Raman spectra of truxene and fluorene. Figures 3 and 4 sketch the molecular normal modes of the main theoretical bands. In the following section Raman spectra of the arms are considered for their bromine derivatives (see Figure 1), assuming that one Br atom occupying one of the two terminal positions of these arms has a negligible influence over the whole molecular conjugation, especially the largest members.

The strongest Raman band of truxene **T0** is measured at 1603 cm^{-1} (calculated: 1600 cm^{-1}) and arises from a CC stretching mode (i.e., mode 8a of benzene[20]) involving exclusively the external benzene rings. In the case of fluorene, this mode appears at 1608 cm^{-1} (calculated: 1602 cm^{-1}). The Raman band of truxene **T0** at 1568 cm^{-1} (calculated: 1558 cm^{-1}) is owing to the same CC stretching mode but located in the innermost benzene ring (i.e., this mode is typical of hexa-substituted benzenes).[20] The doublets at 1608/1580 cm^{-1} in fluorene **F1** and at 1603/1589 cm^{-1} in truxene **T0** display much similarity to the doublet found in oligophenyl oligomers at 1600/1580 cm^{-1} (i.e., Fermi resonance feature), whose I_{1600}/I_{1580} intensity ratio increase is related to efficient conjugation.[21,22] According to this criterion, it is established that fluorene offers better conditions for interannular conjugation than biphenyl (i.e., two phenyl rings connected through a single bond).[22] As for truxene, its I_{1603}/I_{1589} intensity ratio is slightly less than the I_{1600}/I_{1580} one in fluorene. Note that the consideration of the I_{1603}/I_{1568} ratio in truxene is not likely to be a valid argument since it does not correspond to a fundamental/Fermi resonance pair.

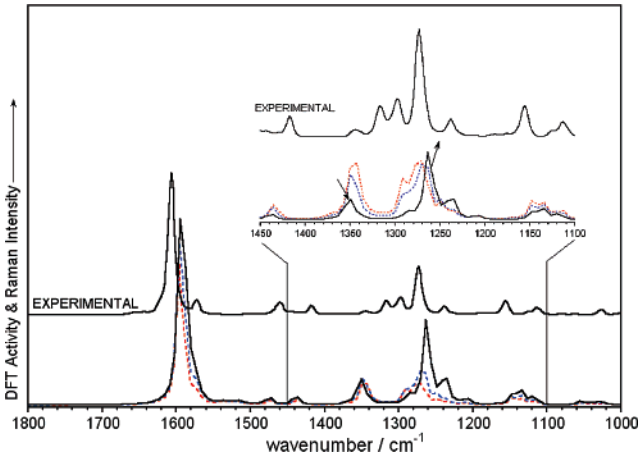

Figure 5. DFT/B3LYP/3-21G* Raman spectrum of the planar conformer of **F2** (bold line, bottom), of the molecule in its optimized geometry (dotted, red lines) and of the conformer with a forced dihedral conformation of 30° (dotted, blue lines). The inset corresponds to the case with the spectra normalized with respect to the β(CH) Raman band, while the normal spectra are displayed as calculated. Arrows in the inset show the evolution of intensity upon planarization.

The group of weak and overlapped bands at 1480−1420 cm^{-1} is likely arising to alkyl CH deformation modes, thus lacking further interest. The most important and distinctive Raman band of the innermost benzene ring of truxene **T0** is detected at 1377 cm^{-1} (calculated: 1378 cm^{-1}) belonging to a symmetric CC stretching mode wherein consecutive CC bonds lengthen and shorten simultaneously. The medium-intensity band at 1295 cm^{-1} (calculated: 1256 cm^{-1}) involves the stretching of the C−C bonds between the benzene rings coupled with the CCC bending modes. As for fluorene **F1**, the medium-weak band at 1342 cm^{-1} (calculated: 1349 cm^{-1}) and the medium-intense line at 1294 cm^{-1} (calculated: 1317 cm^{-1}) might be equally related to combined intra- and inter-ring CC stretches. The weak bands at 1242/1214 cm^{-1} in truxene might be correlated with the weak theoretical band at 1211 cm^{-1} that corresponds to in-plane CH deformation vibrations of the aromatic rings. In fluorene these β(CH) deformations are measured at 1247/1217 cm^{-1} and calculated at 1256/1226 cm^{-1} (see Figures 3 and 4 for the vibrational eigenvectors).

Figure 5 compares the solid-state Raman spectrum of **F2** with that calculated at the B3LYP/3-21G* level (with hexyl groups) for the following cases: (i) the fully planar structure in which the dihedral angle between fluorene groups is forced to 0° (fluorene moieties are disposed in anti conformation whereas the hexyl chains are perpendicular to the fluorene plane and pointing in opposite directions); (ii) the fully optimized geometry, which results in an inter-fluorene distortion angle of 42° (calculations for other fluorene oligomers, i.e., the trimer and pentamer, at the B3LYP/6-31G* level gave optimized geometries with inter-fluorene dihedral angles of 38°);[9e] and finally (iii) a conformer with the two fluorene moieties forced to a dihedral angle of 30°. Figure 6 displays the vibrational eigenvectors associated with the bands that are now discussed. The theoretical feature at 1248 cm^{-1} (i.e., experimental at 1239−1235 cm^{-1}) corresponds to an *in-plane* deformation vibration of the aromatic CH bonds. For this particular mode the CC stretches do not take part at all, a result of importance in the following discussion since this band is taken as a reference for the relative changes of the intensity of the CC modes. A band calculated at 1276 cm^{-1} cm^{-1} a band is calculated (corresponding to the experimental feature at 1274 cm^{-1}), is represented by the stretching of the C−C bond connecting the two fluorene units. As for the predicted band at 1290 cm^{-1} and its weak shoulder at 1305 cm^{-1} (i.e., experimental lines at 1298 and 1317 cm^{-1}), these are due to similar vibrational modes that couple the interfluorene C−C and the intrafluorene C−C stretching bonds (aromatic rings). The intrafluorene C−C stretch of the bond connecting the two benzene rings in fluorene is calculated at 1347 cm^{-1} (experimentally at 1344 cm^{-1}). As can be seen in the eigenvectors, all these vibrations involve, to some extent, the deformation modes of the hexyl chains. However, these alkyl modes are not expected to contribute appreciably to the Raman activity of the C−C/C═C conjugated modes.

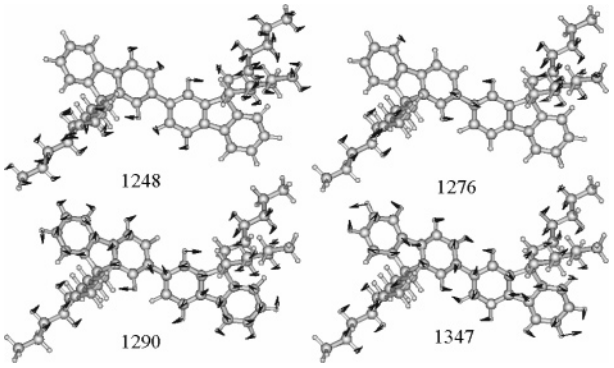

Figure 6. B3LYP/3-21G* theoretical eigenvector for some representative bands of **F2**.

Of the calculated spectra for the different conformers, the planar system better reproduces the experimental Raman spectrum recorded for the solid **F2**. This finding can be explained by assuming that solid-state packing could partially planarize the molecule, a fact supported by the relatively low rotation energy barrier around the C−C inter-fluorene single bond (the total energy difference between the planar and the optimized conformation is 3.35 kcal/mol). The most noticeable feature upon successive lowering of the inter-fluorene distortion angle (i.e., planarization) is the increased intensity for the inter-fluorene ν(C−C) band. Accordingly, one would derive the following: (i) Decreasing/increasing solid-state forces would have an incidence on the molecular spectra, a hypothesis that

TABLE 1: Raman Frequency (cm^{-1}) Correlations and Assignment of the Main Bands Discussed in the Text

F1	F2	assignment	T0	T1	T2	T3	T4	assignment
1608	1607	ν(C═C)	1603	1608	1607	1607	1607	ν(C═C)
1580	1575		1589	1584	1584	1585	1586	
			1568	1563	1562	1560		
			1377	1377	1377	1377	1377	ν(CC)
1342	1344	ν_{intra}(CC) + ν_{inter}(CC)		1343	1340	1344	1345	ν_{inter}(CC)
	1317							
				1311	1309	1307	1306	ν_{inter}(CC)
1294	1298	ν_{inter}(CC) + ν_{intra}(CC)	1295	1294	1292	1291	1291	ν_{inter}(CC)
	1274	ν_{inter}(CC)		1268	1271	1274	1277	ν_{inter}(CC)
1247	1239	β(CH)	1242	1235	1235	1235	1235	β(CH)
1217			1214					

will be addressed in the following sections by discussing the spectra in solution and as a function of temperature. (ii) Increasing conjugation (i.e., planarization) between the fluorene units leads to a selective intensification of the Raman intensity of the inter-fluorene ν(C−C) band. Thus, changes of the molecular structure that would modify inter-fluorene π-conjugation could be monitored by changes of the Raman intensity of this band. Note, furthermore, that in the case of the largest molecules several inter-fluorene stretching modes exist depending on the distance to the core, such that their relative Raman intensities are related to the electronic conjugation between the fluorene units as a function of the branching. This could also be the case of the Raman line associated with the C−C stretching mode of the bond connecting the central core and arms. This interpretation has been already used in the parent oligophenylenes to estimate the efficiency of π-conjugation upon successive planarization of the oligomeric backbone. The main conclusion is that the intensity ratio between the Raman lines of the ν(C−C) around 1280 cm^{-1} and of the β(C−H) at 1220 cm^{-1} can be used as a measure of the planarity, with large I_{1280}/I_{1220} ratios corresponding to effective conjugation.[21,22] Consequently, the relative intensity between the Raman bands involving the C−C stretching of the interfluorene units and the β(C−H) fluorene modes can be taken as a *conjugation parameter*.

Our next step is to attempt a reliable assignment of the bands around 1300 cm^{-1} in the larger samples (**T1**−**T4** in Figure 9), for which Raman spectra calculations cannot be afforded (computationally very expensive). Table 1 summarizes the measured frequencies and establishes an assignment for both the fluorene and truxene series. This correlation is consistent with the whole analysis in the paper, and takes into account the following: (i) It assumes that fluorene units do interact in between and with the core, and likely provoking changes in the relative intensities as a function of the molecular size. This discards the hypothesis of a simple addition of the intensity of individual oscillators to account for the whole of the Raman intensity. (ii) It agrees with the conclusions derived from electronic spectroscopy which show a concomitant red shift of the lowest energy absorption band on going from **T1** to **T4**, indicating sizable electronic interactions among the aromatic subunits. Finally, (iii) it allows a reliable interpretation of the experimental data in the following sections, which show a tuning of the relative intensity between some Raman lines.

If one assumes that the molecular symmetry and vibrational dynamics are essentially unaltered in the truxene series, our argument is that the Raman bands recorded in the 1280−1350 cm^{-1} interval mainly emerge from inter-fluorene ν(C−C) modes of the bonds connecting the successive units and the core. The reassignment of these bands is based on the following: (i) They are particularly intense under conditions of efficient inter-fluorene π-interactions, which is probably the case of the solid state, as observed in **F2** by varying the dihedral angle. (ii) The intra-fluorene modes, also appearing in this interval (see assignment of **F2**) significantly decrease their Raman activity upon planarization. (iii) In experiments where π-electron delocalization between the fluorenes and the truxene is a priori favored, a net intensification of these bands is observed. From another point of view, our hypothesis stems on the existence of different domains for π-electron delocalization depending on the distance to the core. In the following sections, the intensity ratios of the different Raman lines are considered as the quotient between the intensities of each band, measured as the height at the maximum peak wavenumber.

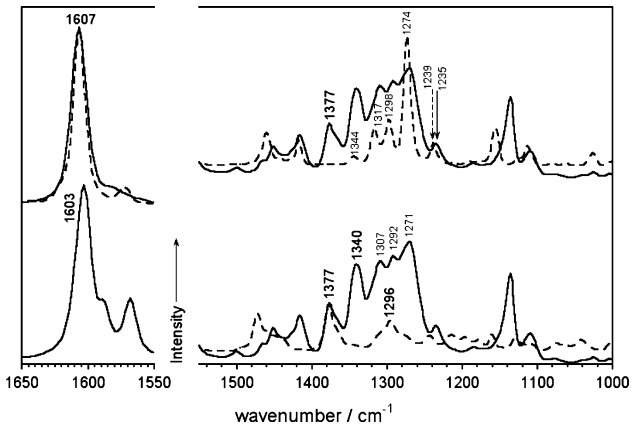

Figure 7. FT-Raman spectra of (upper plot) **F2** in dotted line, **T2** in solid line; and (lower plot) truxene **T0** in dotted line, **T2** in solid line. Spectra are normalized with respect to the bands at 1235−1239 cm^{-1} (top) and 1377 cm^{-1} (bottom).

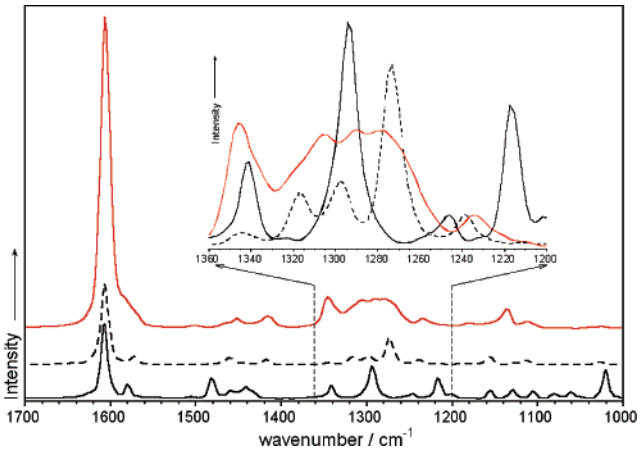

Figure 8. FT-Raman spectra of **F1** (black line), **F2** (dotted line), and **F4** (red line). Inset shows the spectra normalized relative to the 1230−1240 cm^{-1} β(CH) vibration.

III.2. Raman Spectra and the Effect of Branching. Figure 7 displays the FT-Raman spectra of the truxene **T0**, bifluorene **F2**, and **T2**. The spectrum of **T2** is dominated by the Raman scattering of the arms (1607 cm^{-1} in both **F2** and **T2**).

An undistinguished variation of the I_{1600}/I_{1580} ratios is noticed on passing to the branched compound. This agrees with the constant peak position and intensity for the innermost benzene band of the core at 1377 cm^{-1} in truxene **T0** and in **T2**, showing that the interaction is rather limited on the basis of this argument. Conversely, the signal at 1340 cm^{-1} in **T2** is intensified relative to its homologue at 1344 cm^{-1} in bifluorene **F2**. The C−C stretching modes of the bonds connecting the arms to the core are likely involved in this Raman line; therefore, this feature represents the possible channel for electronic interaction of the periphery with the central truxene which might account for the enhanced Raman activity on **F2** → **T2** (1344→1340 cm^{-1}).

We now examine this interaction by considering the relative intensity ratios of the following Raman features: I_{1340}/I_{1235} in **T2** (I_{1344}/I_{1239} in **F2**), I_{1307}/I_{1235} in **T2** (I_{1317}/I_{1239} in **F2**), and I_{1292}/I_{1235} in **T2** (I_{1298}/I_{1239} in **F2**). The ratios are always greater in **T2** than in **F2** for the three lines at higher energies. These differences decrease steadily on going to lower frequencies from 1340 to 1298 cm^{-1}. However, for the I_{1271}/I_{1235} ratio in **T2** and I_{1274}/I_{1239} in **F2**, the intensity ratio is smaller for the truxene derivative. According to the description in section III.1, this latter result can be due to the increased distortion on the outermost periphery of the C_3 molecule compared to **F2** and

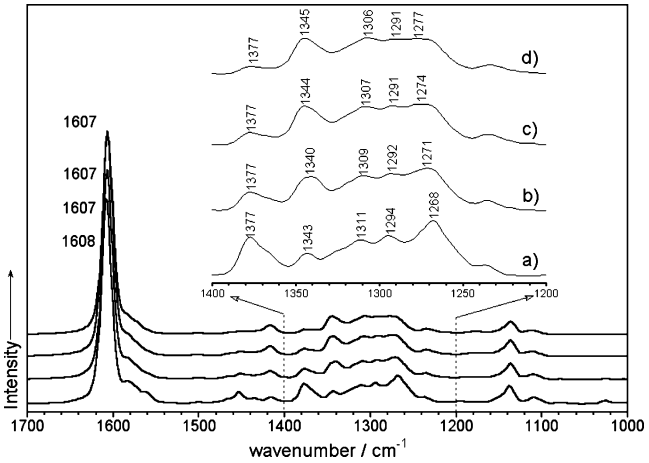

Figure 9. FT-Raman spectra of (a) **T1**, (b) **T2**, (c) **T3**, and (d) **T4**.

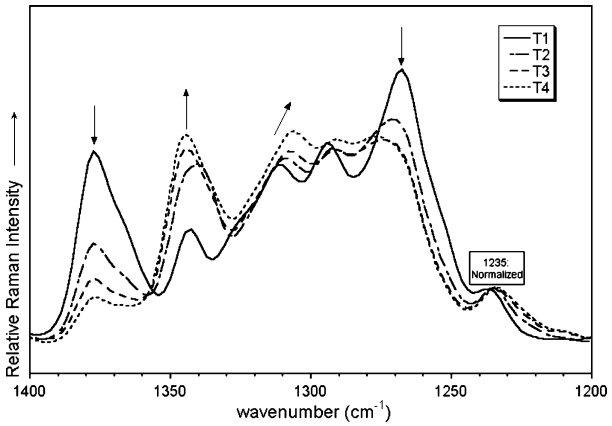

Figure 10. Raman spectra of the trigonal truxene−fluorenes **T1**−**T4** normalized at 1235 cm^{-1}.

the limited degree of conjugation in these external parts of the molecule. Similar behavior is observed upon increasing the chain length within the arms (see Figure 8), namely from fluorene **F1** to bifluorene **F2** and quaterfluorene **F4**. It is well established that, within large linearly conjugated oligomers, π-conjugation takes place more efficiently in the central part of the molecules and decreases toward the ends (terminal or boundary effect).[21,22]

From another point of view, the similarity between the spectra of **F4** and **T4** (section III.3) implies a dominant role of the branches in the description of the molecular features of the trigonal compounds for the longest members of the series (i.e., antenna behavior).

III.3. Raman Spectra of the Trigonal Compounds: Increasing the Arm Length. Figure 9 displays the FT-Raman spectra of the threefold molecules **T0**−**T4** in the whole spectral range, while Figure 10 expands the 1200−1400 cm^{-1} region for normalized spectra. The analysis of the evolution of the I_{1600}/I_{1580} ratio in this series is obscured by the broadening of the strongest band that overlaps both features. As for the two bands at 1563 and 1377 cm^{-1} in **T1**, these are weakened on increasing branching in response to the decreasing statistical weight of the central core.

The intensities of the Raman bands at 1343/1311 cm^{-1} in **T1**, 1340/1309 cm^{-1} in **T2**, 1344/1307 cm^{-1} in **T3**, and 1345/1306 cm^{-1} in **T4** greatly increase relative to the intensity band at 1235 cm^{-1} of each compound with increasing molecular size. This increment is, however, more significant for the higher frequency band which, as already described, could contain an important contribution from ν(C−C) modes located close to the core wherein π-electron delocalization might be particularly

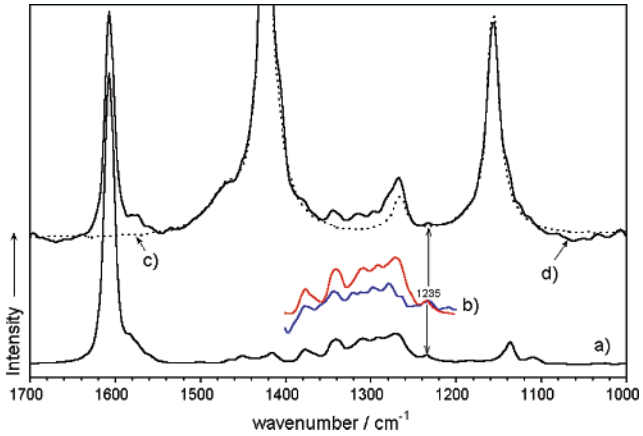

Figure 11. FT-Raman spectra of (a) **T2** in the solid state and (b) **T2** in dichloromethane solution (blue line; the spectrum of the solvent has been subtracted) and in the solid state (red line). These spectra are normalized with respect to the 1235 cm^{-1} band. FT-Raman spectra of (c) pure dichloromethane (dashed line) and (d) **T2** in dichloromethane (the spectrum of the solvent has not been subtracted).

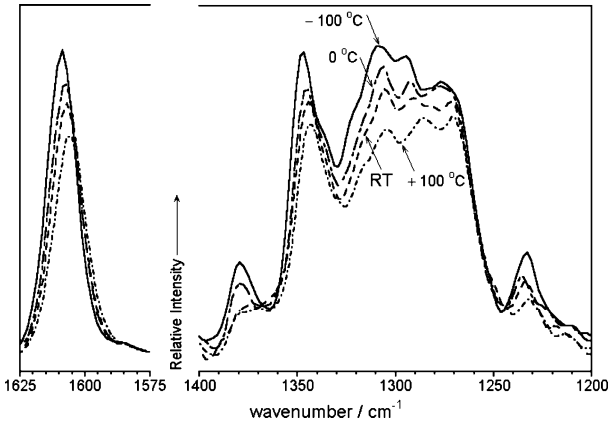

Figure 12. FT-Raman spectra of **T4** as a function of the temperature in solid state.

favored. This behavior reaches the inflection point for the 1294, 1292, 1291, and 1291 cm^{-1} bands in **T1**, **T2**, **T3**, and **T4**, respectively. Again, this is due to the involvement of ν(C−C) modes of the outermost periphery (I_{1268}/I_{1235} in **T1**, I_{1271}/I_{1235} in **T2**, I_{1274}/I_{1235} in **T3**, and I_{1277}/I_{1235} in **T4**).

III.4. Solid-Solution Raman Spectra. Solid-State Packing Forces. Figure 11 compares the Raman spectra of **T2** in dichloromethane and in the solid state. The strongest peak is observed at the same frequency in both spectra. Typical of organic molecules is the displacement of the Raman bands by 4−5 cm^{-1} upon solvation; however, the constant peak in both spectra is in line with a pronounced glassy or amorphous character of these molecules in the solid or thin film states.[23]

However, extra conformational effects due to the removal of packing forces cannot be excluded. If these effects do indeed occur, a reduction of the inter-fluorene and fluorene−truxene interactions and molecular π-electron delocalization might be expected due to increased distortion around C−C single bonds in the liquid phase. This reasoning is highlighted by the observation of a decrease of the I_{1310}/I_{1235}, I_{1294}/I_{1235}, and I_{1270}/I_{1235} ratios upon solvation. A similar effect might be caused by the variation of temperature, since its lowering would promote intermolecular forces (i.e., more contacts) and increased planarization. Figure 12 displays the Raman spectra of **T4** as a function of temperature. It is observed that, upon cooling of the solid material, the ν(C−C) bands involving the innermost

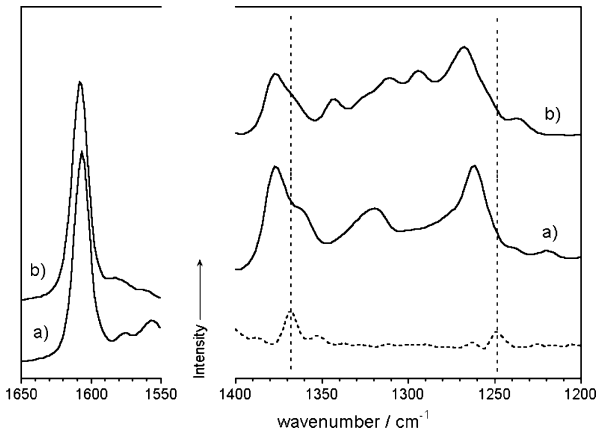

Figure 13. Comparison of the FT-Raman spectra of (a) **Tth2** and (b) **T1**. Dotted line corresponds to the spectrum of 2,2′-bithiophene.

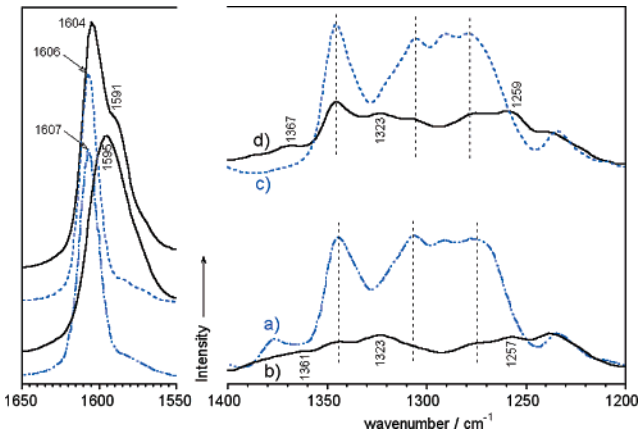

Figure 14. FT-Raman spectra of (a) neutral **T4**, (b) electrochemically oxidized **T4**, (c) neutral **F4**, and (d) electrochemically oxidized **F4**. Each two spectra are normalized relative to the 1235 cm^{-1} band.

connections between the fluorenes and with truxene are particularly intensified.

III.5. Raman Spectra of the Trigonal Compounds: Changing the Type of Arm. Figure 13 shows the FT-Raman spectra of **T1** and a molecule constituted by a central truxene with linear bithiophene arms (**Tth2**), which, similar to **T1**, has two (hetero)-aromatic rings connected to the truxene core. The 1608/1377 cm^{-1} truxene bands are not altered when fluorene arms are replaced by bithiophene, showing the electronic pinning effect due to the aromatization of the central benzene rings.

Comparing the spectrum of **Tth2** to those of the isolated units, no spectral changes due to the interaction between bithiophene and truxene in the 1400−1200 cm^{-1} region are found. The rather different aromatic natures of benzene and thiophene likely restrict electronic interaction relative to the case of interaction between equal units (i.e., thiophene/thiophene or benzene/benzene), such as in the case of fluorene and truxene which both constitute aromatic six-membered rings.

III.6. Raman Spectra of the Trigonal Compounds: Oxidized Species. Figure 14 shows the Raman spectra of **T4** in neutral and oxidized states together with the respective neutral and oxidized spectra of the quaterfluorene derivative **F4**. As for **T4**, oxidation produces the disappearance of the scatterings of the neutral system; this is clearly evidenced for the strongest Raman band that undergoes a 1607→1595 cm^{-1} displacement upon electrochemical treatment. This finding is typical of oligophenylene compounds upon oxidation and relates to the general softening of the molecular structure of the six-membered benzene rings upon electron extraction. This C−C softening consists of their partial aromatic → quinoidal evolution. Oxidation of the quaterfluorene arm leads to a double 1604/1591 cm^{-1} scattering. The differences between these two spectra might highlight the delocalization of the charge defects through the central truxene and only slightly influence the peripheral branches in **T4**.

Assuming that the band around 1235 cm^{-1} is not altered very much upon oxidation (as this band is of β(C−H) nature, while electron extraction alters the CC skeleton), a general weakening of the Raman activity of the single C−C bond skeletal modes is noticed with respect to the neutral species. Oxidation leading to a more quinoidal structure mainly impacts the inter-fluorene and fluorene−truxene dihedral angles due to their planarization. As a result, these C−C bonds should be strengthened and their corresponding Raman frequencies increased. The new oxidized band at 1323 cm^{-1}, likely proceeding from the 1310−1290 cm^{-1} ν(C−C) modes, might corroborate this prediction. The new band at 1361 cm^{-1} can be tentatively originated by the 1345 cm^{-1} ν(C−C) band of the neutral molecule.

IV. Electronic Structures. Frontier Orbitals

It is useful to examine the highest/lowest occupied/virtual molecular orbitals for these compounds because of their relative ordering as a function of the substitution pattern. Such a study might provide a reasonably good indication of the electronic structure in relation to optical properties. To inspect these characteristics, DFT B3LYP/3-21G* calculations of the optimized geometries and of the orbital topologies for representative compounds have been carried out; the results are shown in Figure 15.

IV.1. Electronic Spectra of Truxene and of the Fluorene Building Blocks. Figure 16 compares the UV−vis absorption and emission spectra recorded in dichloromethane for the compounds calculated in Figure 15, which allow us to interpret experimental/theoretical comparisons of energy levels and HOMO−LUMO gaps (i.e., related to the redox gaps). Fluorene derivatives without bromine atoms were not studied experimentally, and although this limits a comparison of the precise wavelength in branched arms, the trends on increasing lengths are comparable between both series.

For truxene, TD-DFT reproduces the appearance of one theoretical transition at 279 nm, with an oscillator strength of 0.41, corresponding to one-electron promotions involving the pairs of π degenerate orbitals (i.e., H − 1 → L, H − 1 → L + 1, H → L, and H → L + 1). These excitations consist of electron transitions among the fluorene moieties of truxene, with the central ring being the overlapping center. In this regard, the electronic absorption spectrum of truxene can be viewed as that of a fluorene, laterally conjugated with two more fused benzenes. This extraconjugation is represented by the red shift of 9 nm from **F1** to **T0**, likely due to the reduction of the HOMO−LUMO gap (i.e., HOMO/LUMO destabilization/stabilization). Both spectra display vibronic resolution resulting from their molecular rigidity. The spectrum of **F2** already lacks this vibronic structure due to the rotation around the single inter-fluorene C−C bond. However, its $\pi-\pi^*$ band is further shifted to the red by 25 nm, resulting from the symmetric reduction of the HOMO−LUMO gap on going from **F1** to **F2**. This finding, also outlined in the previous section of the Raman data, is typical of incremental conjugation upon linear chain elongation within the same series of monomers.

IV.2. Electronic Spectra and the Effect of Branching. TD-DFT calculations for **T1** predict the first dipole-allowed electronic excitation to be $S_0 \rightarrow S_2$ at 354 nm with a very large

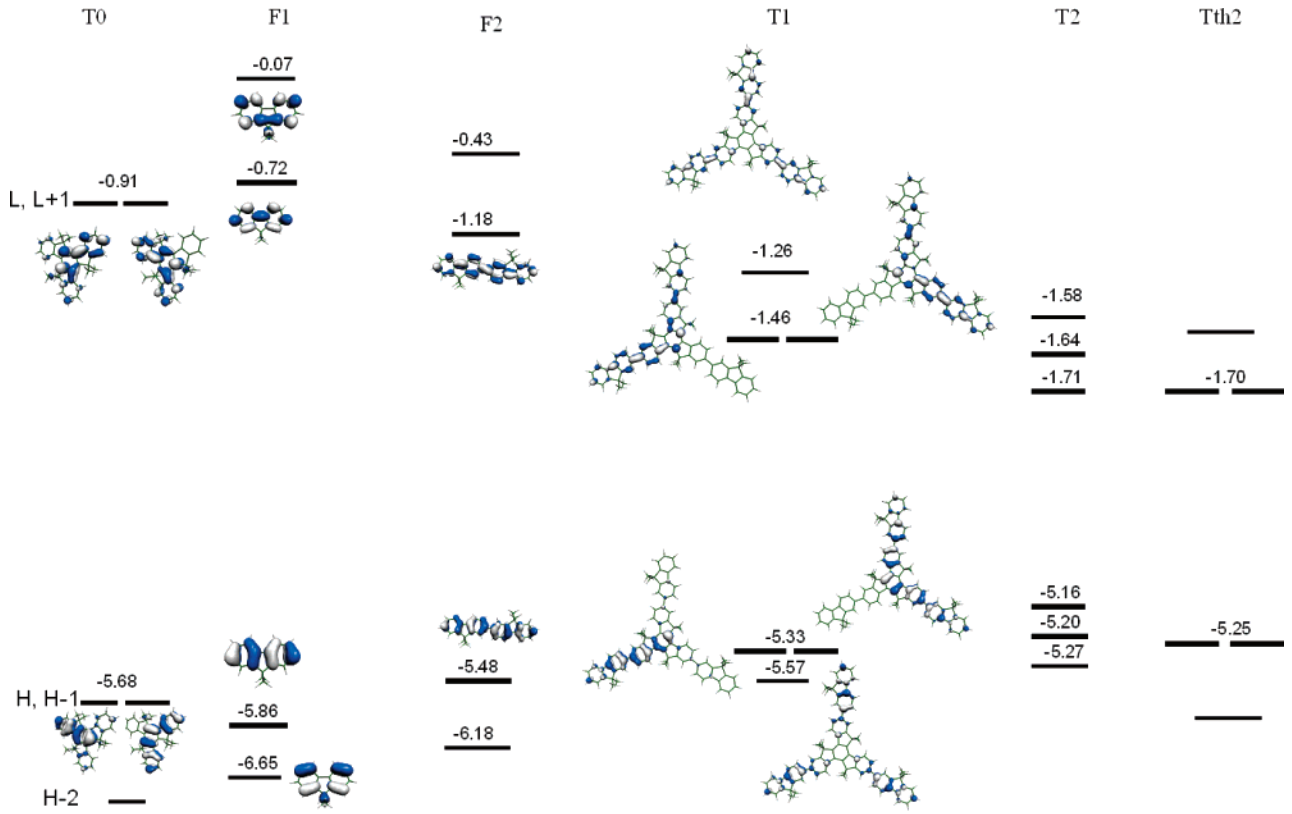

Figure 15. B3LYP/3-21G* energies and topologies of the frontier orbitals around the gap for some representative molecules.

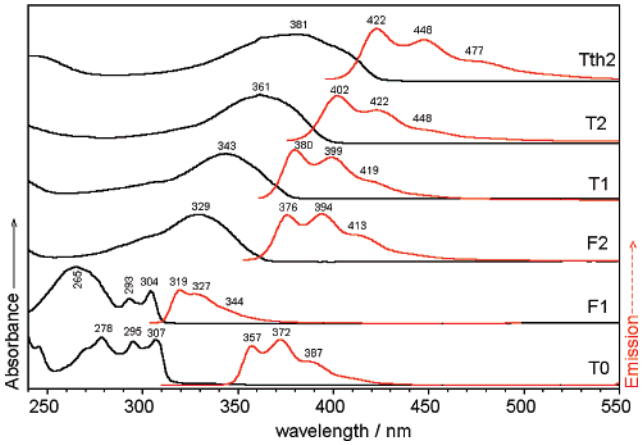

Figure 16. UV−vis absorption and emission spectra in CH_2Cl_2 of some representative molecules. Solutions are prepared in concentrations (10^{-6}−10^{-7} M) giving an absorbance not exceeding 0.1 au.

1.85 oscillator strength ($S_0 \rightarrow S_1$ is a prohibited transition at 364 nm), and that would correspond to the experimental band at 343 nm in **T1**. This $S_0 \rightarrow S_2$ excitation corresponds to the sum of several one-electron promotions (i.e., H − 2 → L, H − 1 → L, H − 1 →L + 1, H → L, H → L + 1 and H → L + 2). According to this theoretical description, fluorescence in these compounds might correspond to the $S_2 \rightarrow S_0$ deactivation channel that, due to its strong coupling with the ground electronic state, might justify their strong fluorescence activity. Threefold substitution of truxene with fluorene arms leads to a 34 nm bathochromic shift of the lowest lying electronic absorption and is accounted for by the stabilization of the LUMO (by 0.55 eV) and destabilization of the HOMO (by 0.35 eV) on **T0** → **T1**. This theoretical result correlates well with the observation of electrochemical reductions and oxidations in these truxene derivatives.[10] The absorption spectrum of **T1** does not show vibronic resolution, which is explained by the incorporation of single C−C bonds, around which rotation is permitted, leading to the appearance of rotamers, especially in solution. This is consistent with the Raman discussion in section III.4.

At the level of the frontier orbitals, the structure of **T1** is reminiscent of that of truxene **T0** with the first two occupied and virtual terms degenerated. The HOMO/HOMO − 1 and LUMO/LUMO + 1 of **T1** spread, in similar extent, over the arms and the outer/central benzene rings of truxene. This situation already changes for the HOMO − 2/LUMO + 2 orbitals mainly located on peripheral arms. This vision is interesting from the point of view of antenna systems operating with gradient energy. Higher energy excitations involving the absorbing arms find a deactivation channel (i.e., $S_n \rightarrow S_2$) that collects the energy toward the core. This representation is very relevant for light-harvesting materials to which highly branched star-shaped or dendrimeric molecules are also conceived.

IV.3. Electronic Spectra of the Trigonal Compounds: Increasing the Arm Length. The wave functions of the orbitals around the gap are increasingly determined by the arms on going from **T1** to **T2**: this is clearly seen in the existence of degeneration in HOMO/HOMO − 1 and LUMO/LUMO + 1 terms in **T1**, which is reminiscent of truxene, while these terms in **T2** are not degenerated anymore, such as in **F2**. Now the topologies of these orbitals in **T2** resemble those of fluorene **F2**. The optical absorption spectrum is red-shifted by 18 nm on **T1** → **T2**, which can be predicted on the basis of the narrowing of the HOMO−LUMO gap with arm elongation. Compared to the **F1** → **F2** evolution (bathochromic shift of 25 nm), branching of the central truxene with the same length arms limits the gap reduction. This is clearly noticed for the destabilization/stabilization of the HOMO/LUMO levels by 0.38/0.46 eV for **F1** → **F2** and 0.17/0.25 eV for **T1** → **T2**. The origin of this behavior is the limiting efficiency of meta

conjugation in this optical excitation, which proceeds between two arms that are connected by meta links through the truxene unit (in contrast to isolated fluorene arms, having para links between the fluorene moieties). Supporting this hypothesis, meta conjugation blocks electron delocalization, especially in the ground-aromatic electronic state (see HOMO/HOMO − 1 wave functions), while in the excited-quinoidal electronic state (see the LUMO/LUMO + 1 wave functions) interaction is favored due to the bonding nature of the C−C bond between the fluorene units and between truxene and fluorene. This bonding feature rigidifies the system, leading to more efficient electron molecular delocalization. As a result, the virtual terms are always more stabilized than the occupied ones.

IV.4. Joint Consideration of Vibrational Raman and Electronic Spectra. In the whole set of compounds, vibrational Raman frequencies are affected only slightly by branching, arm elongation, or substitution (see section III). The origin of this observation probably lies in the minimal changes of their molecular geometries. It is well documented for oligophenylenes that their molecular structures are almost independent of the oligomer size due to electron pinning or strong aromaticity within the six-membered rings (optimized geometries can be provided upon request to the authors).[22] In turn, the evolution of the conjugational properties in these molecules has been assessed based on the changes of the relative Raman intensities (from I_{1300}/I_{1235} ratio, for example). Assuming that Raman activity in these conjugated molecules is mainly dictated by vibronic coupling (i.e., term of pure electronic contribution of the Albrecht theory),[24] the Raman intensity is distributed among the normal modes that better mimic the geometrical changes experienced by the molecules on passing from the aromatic-like structure of the ground electronic state to the quinoidal-like structure of the first dipole accessible excited state. This excitation carries out the largest variation of the dipole moment transitions due to the large oscillator strength, and of molecular polarizability in the presence of an external electric field at the origin of the Raman activity. Part of the important structural reorganization on passing to the quinoidal state occurs within the inter-unit C−C bonds due to the antibonding → bonding change of the charge density. This phenomenon might be more pronounced with increasing number of C−C connecting units as a consequence of (i) the conjugation increment with increasing molecular size and (ii) the Raman enhancement of the ν(C−C) lines as discussed in section III.

IV.5. Electronic Spectra of the Trigonal Compounds: Changing the Type of Arm. Comparing **T1** and **Tth2** a displacement of 20 nm of the strongest absorption band is observed, which is consistent with the reduction of the energy gap predicted by theory. The orbital degeneracy is still maintained in **Tth2**, similar to the case of **T1**. The predicted 0.12/24 eV destabilization/stabilization of the HOMO/LUMO orbitals can be explained by the reduced aromatic character of thiophene, which might lead to a favored electronic delocalization in the LUMO and further facilitated by the electron-donating effect of the sulfur atoms. Indeed, the presence of electron-rich sulfur heteroatoms might disfavor cathodic processes in the truxene−thiophene derivatives in contrast to the truxene−fluorene molecules.

V. Conclusions

In this paper, an analysis is carried out of the molecular and electronic features in a series of threefold molecules constituted by a central truxene unit furnished with three fluorene, bifluorene, terfluorene, and quaterfluorene arms. The main hypothesis is the elucidation of these properties as they evolve from the building block units. Special emphasis is paid to the modulation of conjugation in relation to substitution, molecular dimension and nature, intermolecular forces, oxidation state, etc. Raman spectroscopy and optical absorption/emission spectra in conjunction with computational DFT theory are combined to this end.

The identification of truxene and fluorene Raman bands (i.e., through band assignment guided by DFT calculations), and the estimation of the evolution of the $I_{1340-1270}/I_{1235}$ ratios, as dictated by the electronic interactions among the fluorene units and with the truxene unit, allows us to make a conclusion about the extent of the electronic connection between the core and arms. This interaction is restricted to the outer rings of the truxene core. Conjugation between fluorene units is also found to increase for each two connected units with increasing number of fluorenes, though there is seemingly a saturation of this conjugation due to the increasing propensity toward conformational distortions. Spectroscopic arguments outline the glassy amorphous character of these threefold molecules in the solid state, although the electronic properties are affected by removing solid-state forces or weakening these by increasing temperature. Raman spectra are interpreted on the basis of quinoidization of the molecular structures upon electrochemical oxidation. The introduction of different aromatic rings (fluorene vs thiophene) leads to a very slight change in the ground-state electronic properties (i.e., minimal changes of the Raman spectra and moderate shifts of the HOMO energies). This substitution, however, has a greater effect on the features of the excited states due to the distinct role of the sulfur atoms.

The modulation of optical properties as a function of structure and near-gap energy levels is also interpreted. These experimental/theoretical data are understood in line with the application of these materials: (i) high fluorescence activity and (ii) the design of star-shaped macromolecules pursuing antenna systems. TD-DFT theory is used to assign the main electronic bands to one-electron interorbital promotions. The inversion of the dominance of the truxene features versus those of the fluorene branches is located at the **T1** → **T2** step. It is interesting how certain molecular properties are dominated by the arms or the core, depending on the molecular architecture.

Acknowledgment. J.C. is grateful to the Ministerio de Educación y Ciencia (MEC) of Spain for a I3 research position of Chemistry at the University of Málaga and for funding my stay at the National Research Council of Canada through the fellowship PR2006-0253 of the Programa Nacional de Ayudas a la Movilidad de Profesores e Investigadores en el Extranjero. Research at the University of Málaga was supported by the Ministerio de Educación y Ciencia (MEC) of Spain through the project CTQ2006-14987-C02 and by the Junta de Andalucía (Grant P06-FQM-01678). A.K. thanks the EPRSC (GR/T28379) and R.B. thanks The Leverhulme Trust (F/00120/U) for funding. We thank Professor Jian Pei from the College of Chemistry and Molecular Engineering, Peking University, for providing sample **Tth2**.

References and Notes

(1) *Electronic Materials: The Oligomeric Approach*; Müllen, K., Wegner, G., Eds.; Wiley-VCH: Weinheim, New York, 1998.

(2) (a) Wolffs, M.; Hoeben, F. J. M.; Beckers, E. H. A.; Schenning, A. P. H. J.; Meijer, E. W. *J. Am. Chem. Soc.* **2005**, *127*, 13484−13485. (b) Li, Q.; Jin, C.; Petukhov, P. A.; Rukavishnikov, A. V.; Zaikova, T. O.; Phadke, A.; LaMunyon, D. H.; Lee, M. D.; Keana, J. F. W. *J. Org. Chem.* **2004**, *69*, 1010−1019. (c) Kozaki, M.; Okada, K. *Org. Lett.* **2004**, *6*, 485−488. (d) Nicolas, Y.; Blanchard, P.; Levillain, E.; Allain, M.; Mercier, N.;

Roncali, J. *Org. Lett.* **2004**, *6*, 273−276. (e) Pei, J.; Wang, J.-L.; Cao, X.-Y.; Zhou, X.-H.; Zhang, W.-B. *J. Am. Chem. Soc.* **2003**, *125*, 9944−9945. (f) Meier, H.; Holst, H. C.; Oehlhof, A. *Eur. J. Org. Chem.* **2003**, 4173−4180. (g) Rodríguez, J. G.; Esquivias, J.; Lafuente, A.; Díaz, C. *J. Org. Chem.* **2003**, *68*, 8120−8128. (h) Zhou, X.-H.; Yan, J.-C.; Pei, J. *Org. Lett.* **2003**, *5*, 3543−3546. (i) Li, Q.; Rukavishnikov, A. V.; Petukhov, P. A.; Zaikova, T. O.; Keana, J. F. W. *Org. Lett.* **2002**, *4*, 3631−3634. (j) Kimura, M.; Narikawa, H.; Ohta, K.; Hanabusa, K.; Shirai, H.; Kogayashi, N. *Chem. Mater.* **2002**, *14*, 2711−2717. (k) Cherioux, F.; Guyard, L. *Adv. Funct. Mater.* **2001**, *11*, 305−309.

(3) (a) Yamaguchi, Y.; Ochi, T.; Miyamura, S.; Tanaka, T.; Kobayashi, S.; Wakamiya, T.; Matsubara, Y.; Yoshida, Z.-I. *J. Am. Chem. Soc.* **2006**, *128*, 4504−4505. (b) Li, B.; Xu, X.; Sun, M.; Fu, Y.; Yu, G.; Liu, Y.; Bo, Z. *Macromolecules* **2006**, *39*, 456−461. (c) Lai, W.-Y.; Zhu, R.; Fan, Q.-L.; Hou, L.-T.; Cao, Y.; Huang, W. *Macromolecules* **2006**, *39*, 3707−3709. (d) Sun, M.; Fu, Y.; Li, J.; Bo, Z. *Macromol. Rapid Commun.* **2005**, *26*, 1064−1069. (e) Liu, X.-M.; He, C.; Huang, J.; Xu, J. *Chem. Mater.* **2005**, *17*, 434−441. (f) Li, Z. H.; Wong, M. S.; Tao, Y. *Tetrahedron* **2005**, *61*, 5277−5285. (g) Chou, M.-Y.; Leung, M.-K.; Su, Y. O.; Chiang, C. L.; Lin, C.-C.; Liu, J.-H.; Kuo, C.-K.; Mou, C.-Y. *Chem. Mater.* **2004**, *16*, 654−661. (h) Li, B.; Li, J.; Fu, Y.; Bo, Z. *J. Am. Chem. Soc.* **2004**, *126*, 3430−3431.

(4) (a) Cremer, J.; Bäuerle, P. *J. Mater. Chem.* **2006**, *16*, 874−884. (b) Petrella, A.; Cremer, J.; De Cola, L.; Bäuerle, P.; Williams, R. M. *J. Phys. Chem. A* **2005**, *109*, 11687−11695. (c) de Bettignies, R.; Nicolas, Y.; Blanchard, P.; Levillain, E.; Nunzi, J.-M.; Roncali, J. *Adv. Mater.* **2003**, *15*, 1939−1943.

(5) (a) Ponomarenko, S. A.; Kirchmeyer, S.; Elschner, A.; Huisman, B.-H.; Karbach, A.; Drechsler, D. *Adv. Funct. Mater.* **2003**, *13*, 591. (b) Sun, Y.; Xiao, K.; Liu, Y.; Wang, J.; Pei, J.; Yu, G.; Zhu, D. *Adv. Funct. Mater.* **2005**, *15*, 818−822.

(6) (a) Yan, Y.-X.; Tao, X.-T.; Sun, Y.-H.; Wang, C.-K.; Xu, G.-B.; Yang, J.-X.; Ren, Y.; Zhao, X.; Wu, Y.-Z.; Yu, X.-Q.; Jiang, M.-H. *J. Mater. Chem.* **2004**, *14*, 2995−3000. (b) Brunel, J.; Mongin, O.; Jutand, A.; Ledoux, I.; Zyss, J.; Blanchard-Desce, M. *Chem. Mater.* **2003**, *15*, 4139−4148.

(7) (a) Perepichka, D. F.; Perepichka, I. F.; Meng, H.; Wudl, F. In *Organic Light-Emitting Materials and Devices*; Li, Z. R., Meng, H., Eds.; CRC Press: Boca Raton, FL, 2006; Chapter 2, pp 45−293. (b) Scherf, U.; List, E. J. W. *Adv. Mater.* **2002**, *7*, 477−487. (c) Neher, D. *Macromol. Rapid Commun.* **2001**, *22*, 1365−1385. (d) Leclerc, M. *J. Polym. Sci., Part A: Polym. Chem.* **2001**, *39*, 2867−2873. (e) Bernius, M. T.; Inbasekaran, M.; O'Brien, J.; Wu, W. *Adv. Mater.* **2000**, *12*, 1737−1750.

(8) (a) Grice, A. W.; Bradley, D. D. C.; Bernius, M. T.; Inbasekaran, M.; Wu, W. W.; Woo, E. P. *Appl. Phys. Lett.* **1998**, *73*, 629−631. (b) Redecker, M.; Bradley, D. D. C.; Inbasekaran, M.; Woo, E. P. *Appl. Phys. Lett.* **1998**, *73*, 1565−1567.

(9) (a) Chen, A. C.-A.; Wallace, J. U.; Wei, S. K.-H.; Zeng, L.; Chen, S. H. *Chem. Mater.* **2006**, *18*, 204−213. (b) Schindler, F.; Jacob, J. Grimsdale, A. C.; Scherf, U.; Müllen, K.; Lupton, J. M.; Feldmann, J. *Angew. Chem., Int. Ed.* **2005**, *44*, 1520−1525. (c) Chao, T.-C.; Lin, Y.-T.; Yang, C.-Y.; Hung, T. S.; Chou, H.-C.; Wu, C.-C.; Wong, K.-T. *Adv. Mater.* **2005**, *17*, 992−996. (d) Chi, C.; Im, C.; Enkelmann, V.; Ziegler, A.; Lieser, G.; Wegner, G. *Chem.*−*Eur. J.* **2005**, *11*, 6833−6845. (e) Perepichka, I. I.; Perepichka, I. F.; Bryce, M. R.; Pålsson, L.-O. *Chem. Commun.* **2005**, 3397−3399. (f) Wu, C.-C.; Lin, Y.-T.; Wong, K.-T.; Chen, R.-T.; Chien, Y.-Y. *Adv. Mater.* **2004**, *16*, 61−65. (g) Jo, J.; Chi, C.; Höger, S.; Wegner, G.; Yoon, D. Y. *Chem.*−*Eur. J.* **2004**, *10*, 2681−2688. (h) Güntner, R.; Farrell, T.; Scherf, U.; Miteva, T.; Yasuda, A.; Nelles, G. *J. Mater. Chem.* **2004**, *14*, 2622−2626. (i) Koizumi, Y.; Seki, S.; Acharya, A.; Saeki, A.; Tagawa, S. *Chem. Lett.* **2004**, *33*, 1290−1291. (j) Geng, Y.; Trajkovska, A.; Culligan, S. W.; Ou, J. J.; Chen, H. M. P.; Katsis, D.; Chen, S. H. *J. Am. Chem. Soc.* **2003**, *125*, 14032−14038. (k) Wu, C.-c.; Liu, T.-L.; Hung, W.-Y.; Lin, Y.-T.; Wong, K.-T.; Chen, R.-T.; Chen, Y.-M.; Chien, Y.-Y. *J. Am. Chem. Soc.* **2003**, *125*, 3710−3711. (l) Geng, Y.; Culligan, S. W.; Trajkowska, A.; Wallace, J. U.; Chen, S. H. *Chem. Mater.* **2003**, *15*, 542−549. (m) Geng, Y.; Chen, A. C. A.; Ou, J. J.; Chen, S. H. *Chem. Mater.* **2003**, *15*, 4352−4360. (n) Choi, J.-P.; Wong, K.-T.; Chen, Y.-M.; Yu, J.-K.; Chou, P.-T.; Bard, A. J. *J. Phys. Chem. B* **2003**, *107*, 14407−14413. (o) Geng, Y.; Trajkovska, A.; Katsis, D.; Ou, J. J.; Culligan, S. W.; Chen, S. H. *J. Am. Chem. Soc.* **2002**, *124*, 8337−8347. (p) Wong, K.-T.; Chien, Y.-Y.; Chen, R.-T.; Wang, C.-F.; Lin, Y.-T.; Chiang, H.-H.; Hsieh, P.-Y.; Wu, C.-C.; Chou, C. H.; Su, Y. O.; Lee, G.-H.; Peng, S.-M. *J. Am. Chem. Soc.* **2002**, *124*, 11576−11577. (q) Anémian, R.; Mulatier, J.-C.; Andraud, C.; Stéphan, O.; Vial, J.-C. *Chem. Commun.* **2002**, 1608−1609. (r) Belfield, K. D.; Bondar, M. V.; Morales, A. R.; Yavuz, O.; Przhonka, O. V. *J. Phys. Org. Chem.* **2002**, *16*, 194−201. (s) Lee, S. H.; Nakamura, T.; Tsutsui, T. *Org. Lett.* **2001**, *3*, 2005−2007.

(10) Kanibolotsky, A. L.; Berridge, R.; Skabara, P. J.; Perepichka, I. F.; Bradley, D. D. C.; Koeberg, M. *J. Am. Chem. Soc.* **2004**, *126*, 13695−13702.

(11) (a) Gómez-Lor, B.; de Frutos, Ó.; Ceballos, P. A.; Granier, T.; Echavarren, A. M. *Eur. J. Org. Chem.* **2001**, 2107−2114. (b) Abdourazak, A. H.; Marcinow, Z.; Sygula, A.; Sygula, R.; Rabideau, P. W. *J. Am. Chem. Soc.* **1995**, *117*, 6410−6411. (c) Demlow, E. V.; Kelle, T. *Synth. Commun.* **1997**, *27*, 2021−2031. (d) Plater, M. J.; Praveen, M.; Howie, A. R. *J. Chem. Res., Synop.* **1997**, 46−47; *J. Chem. Res., Miniprint* **1997**, 430−436. (e) Gómez-Lor, B.; de Frutos, Ó.; Echavarren, A. M. *Chem. Commun.* **1999**, 2431−2432. (f) Gómez-Lor, B.; Gonzalez-Cantalapiedra, E.; Ruiz, M.; de Frutos, Ó.; Cardenas, D. J.; Santos, A.; Echavarren, A. M. *Chem.*−*Eur. J.* **2004**, *10*, 2601−2608.

(12) (a) Zhang, X.-R.; Chao, W.; Chuai, Y.-T.; Ma, Y.; Hao, R.; Zou, D.-C.; Wei, Y.-G.; Wang, Y. *Org. Lett.* **2006**, *9*, 2563−2566. (b) Zhang, W.; Cao, X.-Y.; Zi, H.; Pei, J. *Org. Lett.* **2005**, *7*, 959−962. (c) Duan, X.-F.; Wang, J.-L.; Pei, J. *Org. Lett.* **2005**, *7*, 4071−4074. (d) Sánchez, L.; Martín, N.; González-Cantalapiedra, E.; Echavarren, A. M.; Rahman, G. M. A.; Guldi, D. M. *Org. Lett.* **2005**, *8*, 2451−2454. (e) Zheng, Q.; He, G. S.; Prasad, P. N. *Chem. Mater.* **2005**, *17*, 6004−6011. (f) Kimura, M.; Kuwano, S.; Sawaki, Y.; Fujikawa, H.; Noda, K.; Taga, Y.; Takagi, K. *J. Mater. Chem.* **2005**, *15*, 2393−2398. (g) Cao, X.-Y.; Zi, H.; Zhang, W.; Lu, H.; Pei, J. *J. Org. Chem.* **2005**, *70*, 3645−3653. (h) Wang, H.; Wang, J.-L.; Yuan, S.-C.; Pei, J.; Pei, W.-W. *Tetrahedron* **2005**, *61*, 8465−8474. (i) Cao, X.-Y.; Zhou, X.-H.; Zi, H.; Pei, J. *Macromolecules* **2004**, *37*, 8874−8882. (j) Cao, X.-Y.; Zhang, W.; Zi, H.; Pei, J. *Org. Lett.* **2004**. *6*, 4845−4848. (k) Cao, X.-Y.; Zhang, W.-B.; Wang, J.-L.; Zhou, X.-H.; Lu, H.; Pei, J. *J. Am. Chem. Soc.* **2003**, *125*, 12430−12431.

(13) (a) Rumi, M.; Zerbi, G.; Mullen, K.; Muller, G.; Rehahn, M. *J. Chem. Phys.* **1997**, *106*, 24−34. (b) Castiglioni, C.; Del Zoppo, M.; Zuliani, P.; Zerbi, G. *Synth. Met.* **1995**, *74*, 171−177. (c) Rumi, M.; Zerbi, G. *Chem. Phys.* **1999**, *242*, 123. (d) Gussoni, M.; Castiglioni, C.; Zerbi, G. In *Spectroscopy of Advanced Materials*; Clark, R. J., Hester, R. E., Eds.; Wiley: New York, 1991; p 251. (e) Centrone, A.; Brambilla, L.; Renouard, T.; Gherghel, L.; Mathis, C.; Müllen, K.; Zerbi, G. *Carbon* **2005**, *43*, 1593−1609. (f) Castiglioni, C.; López Navarrete, J. T.; Gussoni, M.; Zerbi, G. *Solid State Commun.* **1988**, *65*, 625.

(14) (a) Stephens, P. J.; Devlin, F. J.; Chabalowski, F. C. F.; Frisch, M. J. *J. Phys. Chem.* **1994**, *98*, 11623−11627. (b) Novoa, J. J.; Sosa, C. *J. Phys. Chem.* **1995**, *99*, 15837−15845. (c) Casida, E.; Jamorski, C.; Casida, K. C.; Salahub, D. R. *J. Chem. Phys.* **1998**, *108*, 4439−4449. (d) Stratmann, R. E.; Scuseria, G. E.; Frisch, M. J. *J. Chem. Phys.* **1998**, *109*, 8218−8224.

(15) Frisch, M. J.; Trucks, G. W.; Schlegel, H. B.; Scuseria, G. E.; Robb, M. A.; Cheeseman, J. R.; Montgomery, J. A., Jr.; Vreven, T.; Kudin, K. N.; Burant, J. C.; Millam, J. M.; Iyengar, S. S.; Tomasi, J.; Barone, V.; Mennucci, B.; Cossi, M.; Scalmani, G.; Rega, N.; Petersson, G. A.; Nakatsuji, H.; Hada, M.; Ehara, M.; Toyota, K.; Fukuda, R.; Hasegawa, J.; Ishida, M.; Nakajima, T.; Honda, Y.; Kitao, O.; Nakai, H.; Klene, M.; Li, X.; Knox, J. E.; Hratchian, H. P.; Cross, J. B.; Bakken, V.; Adamo, C.; Jaramillo, J.; Gomperts, R.; Stratmann, R. E.; Yazyev, O.; Austin, A. J.; Cammi, R.; Pomelli, C.; Ochterski, J. W.; Ayala, P. Y.; Morokuma, K.; Voth, G. A.; Salvador, P.; Dannenberg, J. J.; Zakrzewski, V. G.; Dapprich, S.; Daniels, A. D.; Strain, M. C.; Farkas, O.; Malick, D. K.; Rabuck, A. D.; Raghavachari, K.; Foresman, J. B.; Ortiz, J. V.; Cui, Q.; Baboul, A. G.; Clifford, S.; Cioslowski, J.; Stefanov, B. B.; Liu, G.; Liashenko, A.; Piskorz, P.; Komaromi, I.; Martin, R. L.; Fox, D. J.; Keith, T.; Al-Laham, M. A.; Peng, C. Y.; Nanayakkara, A.; Challacombe, M.; Gill, P. M. W.; Johnson, B.; Chen, W.; Wong, M. W.; Gonzalez, C.; Pople, J. A. *Gaussian 03*, revision B.05; Gaussian, Inc.: Wallingford, CT, 2004.

(16) Becke, A. D. *J. Chem. Phys.* **1993**, *98*, 1372−1377.

(17) Francl, M. M.; Pietro, W. J.; Hehre, W. J.; Binkley, J. S.; Gordon, M. S.; Defrees, D. J.; Pople, J. A. *J. Chem. Phys.* **1982**, *77*, 3654−3665.

(18) Scott, A. P.; Radom, L. *J. Phys. Chem.* **1996**, *100*, 16502−16513.

(19) (a) Runge, E.; Gross, E. K. U. *Phys. Rev. Lett.* **1984**, *52*, 997−1000. (b) Gross, E. K. U.; Kohn, W. *Adv. Quantum Chem.* **1990**, *21*, 255−291. (c) Heinze, H.; Goerling, A.; Roesch, N. *J. Chem. Phys.* **2000**, *113*, 2088−2099.

(20) Wilson, E. B.; Decius, J. C.; Cross, P. C. *Molecular Vibrations. The Theory of Infrared and Raman Vibrational Spectra*; McGraw-Hill: New York, Toronto, London, 1955.

(21) (a) Heimel, G.; Somitsch, D.; Knoll, P.; Zojer, E. *J. Chem. Phys.* **2002**, *116*, 10921−10931. (b) Heimel, G.; Somitsch, D.; Knoll, P.; Brédas, J.-L.; Zojer, E. *J. Chem. Phys.* **2005**, *122*, 114511−114519. (c) Guha, S.; Grapner, W.; Resel, R.; Chandrasekhar, M.; Chandrasekhar, R. H.; Glaser, R.; Leising, G. *Phys. Rev. Lett.* **1999**, *82*, 3625−3628. (d) Guha, S.; Rice, J. D.; Martin, C. M.; Grapner, W.; Chandrasekhar, M.; Chandrasekhar, R. H.; Scherf, U. *Mater. Res. Soc. Symp.* **2002**, *708*, BB10.7.1.

(22) (a) Cuff, L.; Kertesz, M.; Scherf, U.; Müllen, K. *Synth. Met.* **1995**, *69*, 683−684. (b) Cuff, L. L.; Cui, C.; Kertesz, M. *J. Am. Chem. Soc.* **1994**, *116*, 9269−9274. (c) Cuff, L.; Kertesz, M. *J. Phys. Chem.* **1994**, *98*, 12223−12231. (d) Cuff, L.; Kertesz, M. *Macromolecules* **1994**, *27*, 762−770.

(23) Reichardt, C. *Solvents and Solvent Effects in Organic Chemistry*, 2nd ed.; VCH-Wiley: Weinheim, 1988.

(24) (a) Long, D. A. *The Raman Effect. An Unified Treatment of the Theory of Raman Scattering by Molecules*; Wiley: Chichester, U.K., 2002. (b) Albrecht, A. C. *J. Chem. Phys.* **1961**, *34*, 1476−1484.